

***L*- and *M*-shell ionization cross sections for 3–40-MeV-proton bombardments**

K. Sera, K. Ishii, and A. Yamadera

Cyclotron and Radioisotope Center, Tohoku University, Sendai 980, Japan

A. Kuwako, M. Kamiya, M. Sebata, and S. Morita

Department of Physics, Faculty of Science, Tohoku University, Sendai 980, Japan

T. C. Chu

Health Physics Division, National Tsing Hua University, Hsinchu, Taiwan 300, Republic of China

(Received 25 February 1980)

Total *L* x-ray production cross sections of Y and Sn and *M* x-ray production cross sections of Au and Bi for proton impact have been measured over the projectile-energy range 3.0–40 MeV and the ionization cross sections obtained for these shells are compared with calculations of the plane-wave Born approximation and the binary encounter approximation. The inner-shell ionizations by close and distant collisions are theoretically discussed in terms of the generalized oscillator strength and the contributions from these two kinds of collisions are separately estimated in the framework of the plane-wave Born approximation. Distant collisions in this energy region are not so effective as in the case of *K*-shell ionization, while at a very high energy the two kinds of collisions contribute nearly equally to the ionization. The experimental results show good agreement with the plane-wave Born approximation calculation except for the *M*-shell ionization of Bi.

I. INTRODUCTION

Inner-shell ionizations by heavy-charged particles can be classified into those by close or hard collisions and by distant or soft collisions. The former one is due to a quasifree scattering between the projectile and an inner-shell electron and the latter is attributed to the photoelectric effect by virtual photons induced by the projectile. Contributions from these two processes depend on the projectile velocity and the state of target electrons. The cross section for inner-shell ionization has been calculated in terms of plane-wave Born approximation (PWBA),¹ and the binary-encounter approximation (BEA),² and semiclassical approximation (SCA).³ The BEA, which takes into account only close collisions, gives the most practical result and is in good agreement with experimental results² in the energy region $E/\lambda U < 1$, where E is the projectile energy, λ is the ratio of the projectile mass to the electron mass, and U is the ionization energy. This fact means that close collisions play a predominant role at the low bombarding energy. In the high-energy region of $E/\lambda U > 1$, however, the BEA predicts that the ionization cross section is smaller than the experimental,^{4,5} and this fact suggests that the contribution from distant collisions might become effective at high energy.

In order to estimate separately the contributions from these two kinds of collisions, measurements of the cross section over a wide range of projectile energy are needed, while the data in the re-

gion $E/\lambda U > 1$ are still scarce.⁴⁻¹⁸ We⁵ have recently measured the *K*-shell ionization cross sections of Al and Cu over the projectile-energy range 0.5–40 MeV and the cross sections were separated into those due to close and distant collisions on the basis of the behavior of the generalized oscillator strength given by PWBA; it was found that the contribution from distant collisions becomes effective in the region $E/\lambda U > 1$ and these two kinds of collisions approximately equally contribute in the region $E/\lambda U > 10$. In this paper, this discussion on ionization mechanism will be extended to the *L*- and *M*-shell ionizations.

Concerning the experimental results on the *L*- and *M*-shell ionization including the energy region $E/\lambda U > 1$, Bissinger *et al.*¹¹ measured the Ag *L*-shell ionization over the energy range $E/\lambda U_L = 0.31$ –4.65, where U_L is the average *L*-shell ionization energy. Watson *et al.*¹² and Hardt *et al.*^{13,14} measured the *L*-shell ionization cross section over the range $E/\lambda U_L = 0.28$ –2.64 on Sn, Te, Nd, Tb, Tm, Au, and Pb. Maeda *et al.*¹⁵ obtained the *L*-shell ionization cross section of Ar over the proton-energy range $E/\lambda U_L = 1.0$ –5.5 from measurements of the Auger electrons. Busch *et al.*¹⁶ measured the *M* x-ray production cross sections of Pb over the proton-energy region $E/\lambda U_M = 0.11$ –2.93. In order to study the contribution from distant collisions, we have here measured the *L* x-ray production cross sections of Y and Sn by proton impact over the energy range $E/\lambda U_L = 0.4$ –10.0 and the *M* x-ray production cross sections of Au and Bi over the range $E/\lambda U_M = 0.541$ –8.44. Poncet

and Engelmann^{17,18} have determined the total L -shell ionization cross sections of Sn and Y over the energy range $E/\lambda U_L = 0.53-7.3$ and also the total M -shell ionization cross sections of Au and Pb over the range $E/\lambda U_M = 0.75-4.637$. In their papers, however, neither the estimation of experimental errors nor the uncertainty of the fluorescence yield used have been mentioned, and we are afraid that there might be large backgrounds from a beam collimator, which is very close to the target. Their results on the M -shell ionization of Pb show substantial deviation from those of Busch *et al.*¹⁶ Thus, we are incapable of evaluating the reliability of their results, and these are not included in the detailed comparison with the present calculation.

The experiment is briefly described in Sec. II. General discussions of the distinction of ionization cross section between those due to close and distant collisions are developed in Sec. III and the results are then applied to the L - and M -shell ionizations. Results of the calculation will be compared with the experimental results in Sec. IV.

II. EXPERIMENTAL

Targets of Y, Sn, Au, and Bi were bombarded with proton beams of 3-40 MeV from the cyclotron of Tohoku University, and the L and M x rays from the targets were measured with a Si(Li) detector. The Y targets of 24 $\mu\text{g}/\text{cm}^2$ was prepared by vacuum evaporating Y onto a 4- μm -thick Mylar foil and the self-supporting targets of Sn, Au, and Bi were of 339-, 282-, and 270- $\mu\text{g}/\text{cm}^2$ thicknesses, respectively, which were determined with an α -ray thickness gauge¹⁹ and from Coulomb scattering of ^3He and deuteron with a Van de Graaff generator. In order to reduce the background due to nuclear γ rays, the target room is separated from the magnet room with 1-m-thick concrete wall and 50-cm thick heavy concrete blocks and the beam was focused on the target without collimator in the target room. After passing through the target, the beam was focused with a pair of quadrupole magnets on the end of a Faraday cup, which is distant by 5.6 m from the target and is shielded with blocks of 100-cm-thick heavy concrete. The detailed experimental arrangement has previously been reported.⁵ The L and M x-ray spectra obtained at $E_p = 40$ MeV, respectively, for Sn and Bi are shown in Fig. 1. The x-ray spectra thus obtained were divided into various x-ray lines by least-squares fitting with a computer assuming Gaussian peaks and a 10th-order polynomial for the background, and after correcting for the detection efficiency, absorption in the air path, and

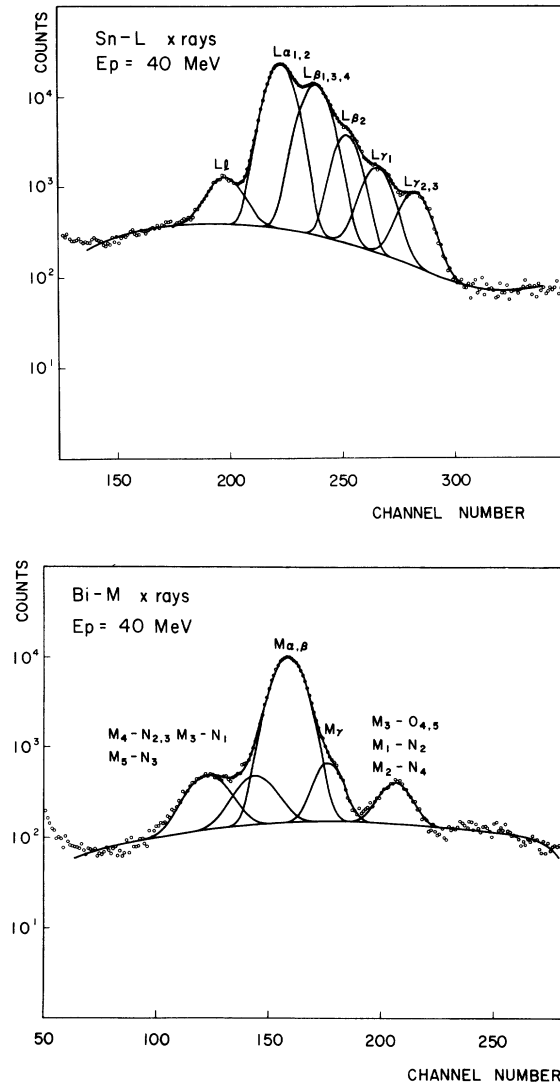


FIG. 1. The L and M x-ray spectra from Sn and Bi targets, respectively, bombarded with 40-MeV protons.

self-absorption for each line, the intensities of each line were summed up, and we obtained the total L - and M - x-ray production cross sections. The results are shown in Table I. The accuracy of these cross sections is estimated to be about 12% from the following errors: background subtraction, 2%; target thickness, 5%; counting statistics, 1%; uncertainty of solid angle, 1%; and the detector efficiency and absorption correction, 11%.

III. THEORETICAL

PWBA and SCA theories include, in principle, ionizations due to both distant and close collisions, and in the SCA calculation, collisions of

TABLE I. Experimental L and M x-ray production cross sections for proton impact (in units of 10^{-22} cm 2). The experimental errors are about 12%.

E_p (MeV)	Y σ_L^X	Sn σ_L^X	Au σ_M^X	Bi σ_M^X
2.92	14.1	8.68	20.3	12.3
3.97	14.9	11.1	23.4	16.2
6.13	14.9	13.7	25.6	16.8
12.31	11.3	14.2	22.9	15.8
18.12	9.37	12.7	19.6	14.4
24.21	8.02	11.0	16.8	11.9
30.52	6.72	9.61	14.6	11.0
39.34	5.37	8.27	11.9	9.49

impact parameter smaller than the orbital radius of electrons to be ionized are regarded as close collisions and those of impact parameter larger than the radius are taken as distant collisions.²⁰ Hence, the contribution from the two kinds of collisions to the ionization can separately be estimated in the SCA and can be compared with experimental results, if the ionization cross section was measured as a function of the impact parameter.

A similar distinction in the PWBA calculation can be done in relation to the integration over the transfer momentum q . As $1/q$ must be an order of magnitude of the domain of collision from the uncertainty principle, the ionization can be considered to be primarily due to close collisions for collisions of $1/q$ smaller than the electronic radius, while distant collisions are predominant for collisions of $1/q$ larger than the atomic radius. However, this separation based on the domain of collisions is not equivalent to a distinction between the ionization mechanisms; the Rutherford scattering between the projectile and the inner-shell electron—close collisions—and the photoelectric effect by virtual photons produced by the projectile—distant collisions. On the basis of the generalized oscillator strength of the PWBA, ionization cross sections for these two ionization mechanisms are separately derived in this section and are applied to L - and M -shell ionizations below.

A. Inner-shell ionization cross section from PWBA

The inner-shell ionization cross section from the nonrelativistic PWBA theory can be calculated by

$$\begin{aligned} \sigma_{n,n'} &= \frac{1}{2\pi} \frac{1}{\hbar^2 v^2} \int q dq \left| \int \psi_n^*(\vec{r}) \frac{ze^2 e^{i\vec{q}\cdot\vec{r}}}{|\vec{R}-\vec{r}|} \psi_n(\vec{r}) d\vec{r} d\vec{R} \right|^2 \\ &= 8\pi z^2 \left(\frac{e^2}{\hbar v} \right)^2 \int \frac{dq}{q^3} \left| \int \psi_n^* e^{i\vec{q}\cdot\vec{r}} \psi_n d\vec{r} \right|^2, \end{aligned} \quad (1)$$

where $\hbar q$ is the transfer momentum of the projectile, v is the projectile velocity, z is the projectile-charge number, and n and n' are, respectively, the initial and final states of the electron. By doing sums on the final state in Eq. (1), the total cross section for inner-shell ionization is obtained by

$$\sigma_n = 8\pi z^2 \frac{a_0^2}{z_s^4} \frac{1}{\eta} \int_{W_{\min}}^{\infty} \frac{dW}{W} \int_{Q_{\min}}^{\infty} \frac{dQ}{Q} F_n(W, Q), \quad (2)$$

where

$$\begin{aligned} Q &= \frac{\hbar^2 q^2}{2m} \frac{1}{z_s^2 \text{Ry}}, \quad \eta = \frac{m}{M} \frac{E}{z_s^2 \text{Ry}}, \\ Q_{\min} &= \frac{W^2}{4\eta}, \quad \text{and } W_{\min} = \theta/n^2, \end{aligned}$$

and Z_s is the effective atomic number of the target nucleus for the electron, and M and E are the mass and incident energy of the projectile, respectively. Further, W is the transfer energy of the projectile measured in units of $Z_s^2 \text{Ry}$, and θ is the screening constant.^{1,21} The transfer energy W is related to the wavelength k of the ionized electron in the final state by

$$W = k^2 + 1/n^2, \quad (3)$$

where k is measured in units of Z_s/a_0 . The final state is expressed by k hereafter. The quantity $F_n(W, Q)$ in Eq. (2) is defined by

$$F_n(W, Q) = (2l_n + 1) \frac{W}{Q} \int \frac{d\Omega_{\vec{k}}}{4\pi} \left| \int \psi_k^* e^{i\vec{q}\cdot\vec{r}} \psi_n d\vec{r} \right|^2, \quad (4)$$

and is called the generalized oscillator strength.²²

B. Generalized oscillator strength

Behavior of the generalized oscillator strength in the space of transferred momentum-transferred energy is characterized by the Bethe surface²³; in the region of low transferred momentum, $F_n(W, Q)$ is flat, while in the region of high transferred momentum, it has a peak at $Q \approx W$, which is known as the Bethe ridge. This behavior in the two extreme cases reflects the two kinds of collisions and can be understood as follows.

The generalized oscillator strength for low transferred momentum of $qr \ll 1$ corresponds to the collision between the projectile and the cloud of inner-shell electrons, and the dipole approximation can be applied to Eq. (4) by

$$F_n(W, 0) = \frac{2m}{\hbar^2} W \int \frac{d\Omega_{\vec{k}}}{4\pi} \left| \int \psi_k^* z \psi_n d\vec{r} \right|^2, \quad (5)$$

namely, $F_n(W, Q)$ is just the optical oscillator strength and becomes flat independently of Q .

Hence, the ionization in this region is due to the virtual photoelectric effect, distant collisions.

On the other hand, the domain of collision is much smaller than the cloud of inner-shell electrons for a high-momentum transfer of $qr \gg 1$ and the inner-shell electrons can be regarded as free, since the change $\delta V_c/V_c$ of the Coulomb field V_c of the target nucleus in the collision domain can be neglected because of $\delta V_c/V_c \approx 1/qr$, so that the Coulomb field can be assumed to be constant in the collision domain. For such an impulse approximation, Eq. (4) can be modified by²⁴

$$F_n^{\text{BEA}}(W, Q) = (2l_n + 1) \frac{W}{2Q} \frac{Ry}{\hbar q} \int_{\frac{2Ry}{\hbar q}}^{\infty} f_n(v) \frac{dv}{v} \quad (6)$$

Here $f_n(v)$ is the velocity distribution of electrons in the initial state and l_n is the azimuthal quantum number. The superscript BEA means that the BEA theory is based on Eq. (6). The value of $F_n^{\text{BEA}}(W, Q)$ becomes maximum at $Q = W$, which corresponds to the Bethe ridge. It has also been shown²⁴ that $F_n^{\text{BEA}}(W, Q)$ given by Eq. (6) is in good agreement with $F_n(W, Q)$ given by Eq. (4) in the region of $Q \geq W$.

It is thus possible for us to try to separate the exact form $F_n(W, Q)$ given by Eq. (4) into the approximate generalized oscillator strength $F_n^{\text{CC}}(W, Q)$ corresponding to close collisions and that $F_n^{\text{DC}}(W, Q)$ corresponding to distant collisions over the whole range of the transfer momentum as expressed by

$$F_n(W, Q) = F_n^{\text{CC}}(W, Q) + F_n^{\text{DC}}(W, Q). \quad (7)$$

For this purpose, $F_n(W, Q)$ is divided into two parts on the basis of $F_n^{\text{BEA}}(W, Q)$ given by Eq. (6) and $F_n(W, Q)$ given by Eq. (5). The function $F_n^{\text{BEA}}(W, Q)$ is considered to have the character of the generalized oscillator strength of close collisions over the whole range of the transfer momentum, since Eq. (6) is derived from Eq. (4) which is based only on the free-electron assumption—the close collisions. Using the velocity distribution function $f_n(v)$ derived from a hydrogenlike wave function, Eq. (6) can be expressed by

$$F_n^{\text{BEA}}(W, Q) = \frac{2^3}{\pi} W Q^{1/2} \left[(W - Q)^2 + \left(\frac{2}{n}\right)^2 Q \right]^{-(2n+1)} \times \sum_j [B_j^n(Q)(W - Q)^j], \quad (8)$$

where $B_j^n(Q)$ is a polynomial of Q . On the other hand, $F_n(W, Q)$ of Eq. (4) can generally be expressed by

$$F_n(W, Q) = 2^4 W \frac{\exp\left(-\frac{2}{k} \tan^{-1} \frac{2k/n}{Q - W + 2/n^2}\right)}{1 - \exp(-2\pi/k)} \times \left[(W - Q)^2 + \left(\frac{2}{n}\right)^2 Q \right]^{-(2n+1)} \times \sum_j [A_j^n(Q)(W - Q)^j], \quad (9)$$

where $A_j^n(Q)$ is a polynomial of Q .

Equations (8) and (9) have already been successfully applied to K - and L -shell ionizations,^{5,24} and will be proved to hold for M -shell ionizations below. The factors in Eqs. (8) and (9), respectively, $Q^{1/2}/2\pi$ and $\exp\{-\frac{2}{k} \tan^{-1}[(2k/n)/(Q - W + 2/n^2)]\}/[1 - \exp(-2\pi/k)]$ agree with each other under the conditions of $W = Q$ and $k \gg 1$, and slowly change depending on Q . Hence, the factor $A_j^n(Q)$ in Eq. (9) is to be compared with $B_j^n(Q)$ in Eq. (8). Using the asymptotic solution²⁵ of $f_n(v)$ for a high velocity v in Eq. (6), $F_n^{\text{BEA}}(W, Q)$ for small Q can be expressed by

$$F_n^{\text{BEA}}(W, Q) \approx \text{const} Q^{1/2} Q^{l+1}, \quad (10)$$

where l is the quantum number of the angular momentum. Making a comparison between Eqs. (8) and (10), we obtain $B_j^n(0) = 0$. Thus the part corresponding to close collisions in $F_n(W, Q)$ of Eq. (9) must be $A_j^n(Q)$, which becomes $A_j^n(0) = 0$, while the part corresponding to distant collisions can approximately be taken as $A_j^n(0)$ from the derivation of Eq. (5). As a result, we can divide $A_j^n(Q)$ into $A_j^n(Q) - A_j^n(0)$ and $A_j^n(0)$, corresponding to close and distant collisions, respectively, and consequently, $F_n(W, Q)$ can be divided into the two parts as expressed by

$$F_n^{\text{CC}}(W, Q) = 2^4 W \frac{\exp\left(-\frac{2}{k} \tan^{-1} \frac{2k/n}{Q - W + 2/n^2}\right)}{1 - \exp(-2\pi/k)} \times \left[(W - Q)^2 + \left(\frac{2}{n}\right)^2 Q \right]^{-(2n+1)} \times \sum_j \{ [A_j^n(Q) - A_j^n(0)] (W - Q)^j \}, \quad (11)$$

and

$$F_n^{\text{DC}}(W, Q) = 2^4 W \frac{\exp\left(-\frac{2}{k} \tan^{-1} \frac{2k/n}{Q - W + 2/n^2}\right)}{1 - \exp(-2\pi/k)} \times \left[(W - Q)^2 + \left(\frac{2}{n}\right)^2 Q \right]^{-(2n+1)} \times \sum_j [A_j^n(0)(W - Q)^j]. \quad (12)$$

It has been confirmed²¹ that $F_n^{\text{BEA}}(W, Q)$ given by Eq. (6) gives good agreement with the exact

$F_n(W, Q)$ in the region $Q \gg W$. Hence $F_n^{\text{DC}}(W, Q)$ can be neglected in this region, and we obtain

$$F_n^{\text{CC}}(W, Q) = F_n(W, Q), \quad (13)$$

and

$$F_n^{\text{DC}}(W, Q) = 0, \quad \text{for } Q \geq W.$$

From $F_n^{\text{CC}}(W, Q)$ and $F_n^{\text{DC}}(W, Q)$ thus obtained and from Eq. (2), we can separately calculate the ionization cross sections for close and distant collisions. Besides the result on the K -shell ionization,⁵ calculations for L - and M -shell ionization are reported here.

C. L -shell ionizations

L -shell ionization cross sections have been calculated in terms of PWBA by Choi,^{26,27} and by Benka and Kropf.²⁸ From these results, the functions $F_n(W, Q)$ for electrons in the $2s$ and $2p$ states are obtained by

$$F_{2s}(W, Q) = A(W, Q)B(W, Q) \sum_{j=0}^5 [A_j^{2s}(Q)(W-Q)^j] \quad (14)$$

and

$$F_{2p}(W, Q) = A(W, Q)B(W, Q) \sum_{j=0}^4 [A_j^{2p}(Q)(W-Q)^j], \quad (15)$$

where

$$A(W, Q) = 2^4 W \frac{\exp\left(-\frac{2}{k} \tan^{-1} \frac{k}{Q-W+1/2}\right)}{1 - \exp(-2\pi/k)}, \quad (16)$$

$$B(W, Q) = [(W-Q)^2 + Q]^{-5}.$$

The coefficients $A_j^{2s}(Q)$ are given by

$$\begin{aligned} A_0^{2s}(Q) &= \left(\frac{19}{60} + \frac{8}{15}Q\right)Q^2, \\ A_1^{2s}(Q) &= \frac{1}{15}(Q+1)Q, \\ A_2^{2s}(Q) &= \frac{1}{30}(1-40Q)Q, \\ A_3^{2s}(Q) &= \frac{2}{3}Q, \\ A_4^{2s} &= \frac{1}{4} + \frac{4}{3}Q, \\ A_5^{2s}(Q) &= \frac{1}{3}. \end{aligned} \quad (17)$$

Similarly, $A_j^{2p}(Q)$ are given by

$$\begin{aligned} A_0^{2p}(Q) &= \left(\frac{17}{12} + \frac{4}{5}Q\right)Q^2, \\ A_1^{2p}(Q) &= \left(\frac{1}{10} + \frac{34}{15}Q\right)Q, \\ A_2^{2p}(Q) &= \frac{1}{30}(49+120Q)Q, \\ A_3^{2p}(Q) &= \frac{1}{6} + 2Q, \\ A_4^{2p}(Q) &= \frac{1}{4}. \end{aligned} \quad (18)$$

On the other hand, the generalized oscillator strengths for the $2s$ and $2p$ states in terms of the impulse approximation are calculated from Eq. (6) using hydrogenlike wave functions in the momentum representation by²⁴

$$F_{2s}^{\text{BEA}}(W, Q) = \frac{2^3}{\pi} W Q^{1/2} [(W-Q)^2 + Q]^{-5} \times \sum_{j=0,2,4} [B_j^{2s}(Q)(W-Q)^j], \quad (19)$$

$$F_{2p}^{\text{BEA}}(W, Q) = \frac{2^3}{\pi} W Q^{1/2} [(W-Q)^2 + Q]^{-5} \times \sum_{j=0,2} [B_j^{2p}(Q)(W-Q)^j], \quad (20)$$

where $B_j^n(Q)$ are given by

$$\begin{aligned} B_0^{2s}(Q) &= \frac{8}{15}Q^3, \\ B_2^{2s}(Q) &= -\frac{4}{3}Q^2, \\ B_4^{2s}(Q) &= \frac{4}{3}Q, \\ B_0^{2p}(Q) &= \frac{4}{5}Q^3, \\ B_2^{2p}(Q) &= 4Q, \end{aligned} \quad (21)$$

and, for odd j ,

$$B_j(Q) = 0.$$

In comparison of Eqs. (17) and (18) with Eq. (21), we can find in $A_j^n(Q)$ a term corresponding to $B_j^n(Q)$. The functions $F_n(W, Q)$ given by Eq. (15) and $F_n^{\text{BEA}}(W, Q)$ given by Eq. (20) are plotted in Fig. 2 as a function of transfer momentum Q with

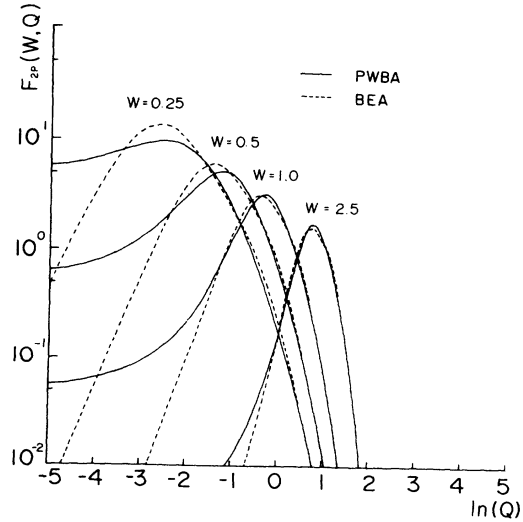


FIG. 2. Comparisons of the generalized oscillator strengths for $2p$ -state ionization between the PWBA and the BEA. The generalized oscillator strength is shown as a function of logarithm of transfer momentum Q . The transfer energy W is taken as a parameter.

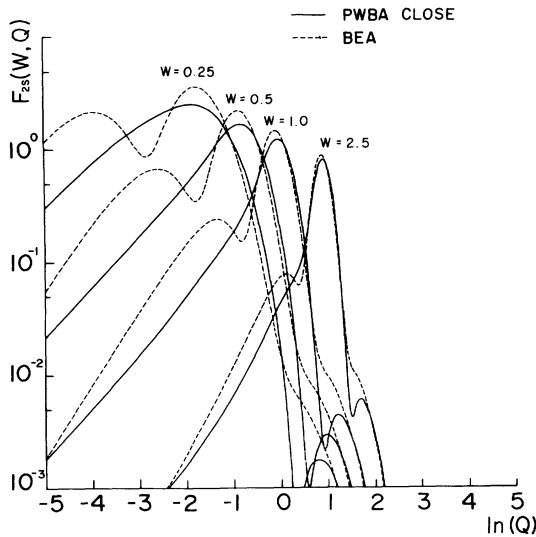


FIG. 3. Generalized oscillator strengths for $2s$ -state ionization by close collisions in the PWBA, estimated from Eq. (11), are compared with those of the BEA.

a parameter of transfer energy W . As seen in this figure, $F_n(W, Q)$ agrees well with $F_n^{\text{BEA}}(W, Q)$ in the region $Q \geq W$, and $F_n^{\text{BEA}}(W, Q)$ rapidly decreases with a decrease in Q . The situation is same for the $2s$ state. As are shown in Figs. 3 and 4, the functions $F_n^{\text{CC}}(W, Q)$ given by Eq. (11) approximately agree with $F_n^{\text{BEA}}(W, Q)$. It is thus shown that the separation method described in the preceding section is applicable to L -shell ionizations.

The functions $F_n^{\text{CC}}(W, Q)$ and $F_n^{\text{DC}}(W, Q)$ given by Eqs. (11) and (12), together with $F_n(W, Q)$, are shown in Figs. 5 and 6, respectively, for $2s$ and

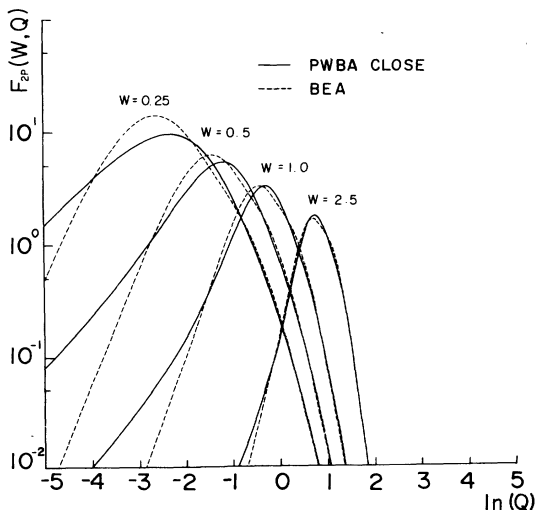


FIG. 4. Same as Fig. 3, except for the $2p$ state.

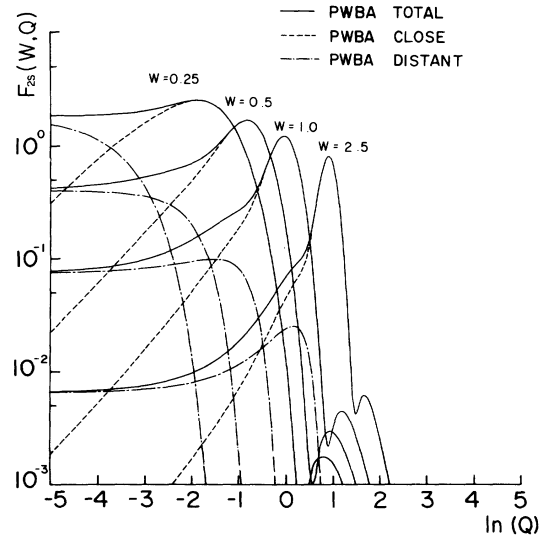


FIG. 5. The generalized oscillator strengths $F_{2s}(W, Q)$ for $2s$ -state ionization from the PWBA—solid lines—are decomposed into dashed lines $F_{2s}^{\text{CC}}(W, Q)$ for close collisions and dash-dot lines $F_{2s}^{\text{DC}}(W, Q)$ for distant collisions in accordance with Eqs. (7), (11), and (12).

$2p$ states. Since the $2s$ -state wave function has a node, $F_{2s}(W, Q)$ has structure. As can be seen in Fig. 5, however, the ionization cross section due to distant collisions does not reflect this structure. We can thus obtain the ionization cross sections of $2s$ and $2p$ states separately for close and distant collisions in conformity with Eqs. (2) and (11)–(15). The total L x-ray production cross sections for Y and Sn, thus calculated, are illustrated as a function of incident energy in Figs. 7 and 8 together with the present experimental results. In these figures, the total L -x-ray produc-

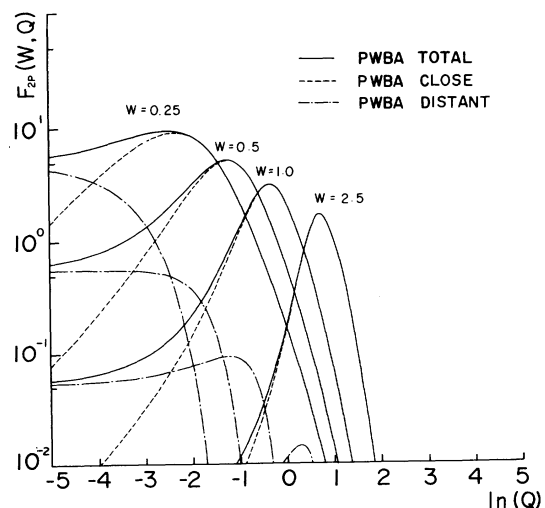


FIG. 6. Same as Fig. 5, except for the $2p$ state.

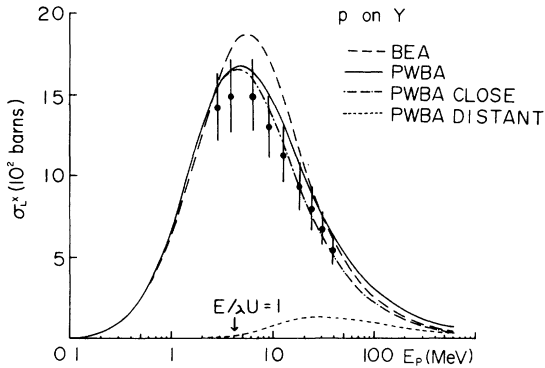


FIG. 7. The total L x-ray production cross sections of Y for proton impact are compared with the PWBA calculation (the solid line) and the BEA (the dashed line). The dot-dash line and the dotted line are, respectively, the PWBA cross sections decomposed into those for close collisions and those for distant collisions.

tion cross section σ_{Lx}^T , the contribution from close collisions σ_{Lx}^{CC} , and that from distant collisions σ_{Lx}^{DC} , are calculated by

$$\begin{aligned}\sigma_{Lx}^{CC} &= \sum_{i=1}^3 \omega_i^{\text{eff}} \sigma_i^{CC}, \\ \sigma_{Lx}^{DC} &= \sum_{i=1}^3 \omega_i^{\text{eff}} \sigma_i^{DC}, \\ \sigma_{Lx}^T &= \sigma_{Lx}^{CC} + \sigma_{Lx}^{DC},\end{aligned}\quad (22)$$

where

$$\begin{aligned}\omega_1^{\text{eff}} &= \omega_1 + f_{12}\omega_2 + (f_{13} + f_{12}f_{23})\omega_3, \\ \omega_2^{\text{eff}} &= \omega_2 + f_{23}\omega_3,\end{aligned}\quad (23)$$

and

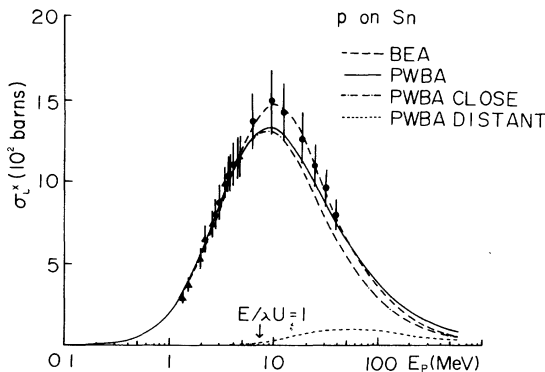


FIG. 8. Same as Fig. 7, except for Sn . The circles represent the present data and the triangles show the previous experimental results of Ref. 34.

$$\omega_{\text{eff}}^3 = \omega_3.$$

The subscripts 1, 2, and 3 stand for the L -shell substates L_I , L_{II} , and L_{III} , respectively. The cross sections σ_i^{CC} and σ_i^{DC} are the subshell-ionization cross sections calculated from Eq. (2) and Eqs. (11)–(15). The notations ω_i and f_{ik} are, respectively, the fluorescence yield and the Coster-Kronig transition probability, and were taken from a table of Bambynek *et al.*²⁹ It is seen from the figures that the contribution from distant collisions becomes effective in the region $E/\lambda U > 1$, but not so remarkable as in the case of K -shell ionization.⁵ At very high proton energy beyond the experimental points, the contribution from distant collisions becomes nearly equal to that from close collisions.

D. M -shell ionizations

In conformity with the PWBA calculation of Choi²¹ for M -shell ionizations, the generalized oscillator strengths for the $3s$, $3p$, and $3d$ states are given by

$$F_{3s}(W, Q) = A(W, Q)B(W, Q) \sum_{j=0}^9 [A_j^{3s}(Q)(W-Q)^j], \quad (24)$$

$$F_{3p}(W, Q) = A(W, Q)B(W, Q) \sum_{j=0}^8 [A_j^{3p}(Q)(W-Q)^j], \quad (25)$$

$$F_{3d}(W, Q) = A(W, Q)B(W, Q) \sum_{j=0}^7 [A_j^{3d}(Q)(W-Q)^j], \quad (26)$$

where

$$\begin{aligned}A(W, Q) &= 2^4 W \frac{\exp\left(-\frac{2}{k} \tan^{-1} \frac{\frac{2}{3}k}{Q - W + \frac{2}{9}}\right)}{1 - \exp(-2\pi/k)}, \\ B(W, Q) &= [(W-Q)^2 + \frac{4}{9}Q]^{-7},\end{aligned}\quad (27)$$

with

$$W = k^2 + \frac{1}{9}.$$

The coefficients $A_j^{3s}(Q)$, A_j^{3p} , and $A_j^{3d}(Q)$ are given by

$$\begin{aligned}
& A_j^{3s}(Q): \\
A_0^{3s}(Q) &= \left(\frac{528\,384}{502\,211\,745} + \frac{561\,152}{55\,801\,305} Q \right. \\
& \quad \left. + \frac{68\,608}{6\,200\,145} Q^2 \right) \frac{2^3}{3^3} Q^3, \\
A_1^{3s}(Q) &= \left(\frac{32\,768}{167\,403\,915} + \frac{2048}{413\,343} Q \right. \\
& \quad \left. - \frac{7424}{6\,200\,145} Q^2 \right) \frac{2^3}{3^3} Q^2, \\
A_2^{3s}(Q) &= \left(\frac{8192}{6\,200\,145} - \frac{63\,488}{1\,240\,029} Q - \frac{17\,408}{98\,415} Q^2 \right) \frac{2^3}{3^3} Q^2, \\
A_3^{3s}(Q) &= \left(\frac{256\,768}{6\,200\,145} + \frac{256}{729} Q \right) \frac{2^4}{3^3} Q^2, \\
A_4^{3s}(Q) &= \left(\frac{11\,008}{885\,735} + \frac{30\,976}{98\,415} Q + \frac{15\,744}{10\,935} Q^2 \right) \frac{2^3}{3^3} Q, \\
A_5^{3s}(Q) &= \left(\frac{2816}{32\,805} - \frac{10\,912}{10\,935} Q \right) \frac{2^3}{3^3} Q, \\
A_6^{3s}(Q) &= \left(\frac{128}{19\,683} + \frac{1024}{10\,935} Q - \frac{64}{27} Q^2 \right) \frac{2^3}{3^3}, \\
A_7^{3s}(Q) &= \left(\frac{208}{2187} + \frac{80}{81} Q \right) \frac{2^3}{3^3}, \\
A_8^{3s}(Q) &= \left(\frac{32}{81} + \frac{4}{3} Q \right) \frac{2^3}{3^3}, \\
A_9^{3s}(Q) &= \frac{1}{3} \frac{2^3}{3^3}, \\
& A_j^{3p}(Q); \\
A_0^{3p}(Q) &= \left(\frac{495\,616}{167\,403\,915} + \frac{443\,392}{18\,600\,435} Q \right. \\
& \quad \left. + \frac{8192}{413\,343} Q^2 \right) \frac{2^3}{3^3} Q^3, \\
A_1^{3p}(Q) &= \left(\frac{65\,536}{167\,403\,915} + \frac{546\,304}{18\,600\,435} Q \right. \\
& \quad \left. + \frac{38\,912}{413\,343} Q^2 \right) \frac{2^3}{3^3} Q^2, \\
A_2^{3p}(Q) &= \left(\frac{274\,944}{18\,600\,435} + \frac{135\,424}{2\,066\,715} Q + \frac{2048}{6561} Q^2 \right) \frac{2^3}{3^3} Q^2, \\
A_3^{3p}(Q) &= \left(\frac{4096}{2\,657\,205} + \frac{15\,872}{137\,781} Q - \frac{22\,528}{32\,805} Q^2 \right) \frac{2^3}{3^3} Q, \\
A_4^{3p}(Q) &= \left(\frac{512}{32\,805} + \frac{2368}{10\,935} Q - \frac{512}{243} Q^2 \right) \frac{2^3}{3^3} Q, \\
A_5^{3p}(Q) &= \left(\frac{8992}{32\,805} + \frac{1664}{729} Q \right) \frac{2^3}{3^3} Q, \\
A_6^{3p}(Q) &= \left(\frac{224}{6561} + \frac{560}{243} Q + \frac{128}{27} Q^2 \right) \frac{2^3}{3^3}, \\
A_7^{3p}(Q) &= \left(\frac{208}{729} + \frac{64}{27} Q \right) \frac{2^3}{3^3}, \\
A_8^{3p}(Q) &= \frac{8}{27} \frac{2^3}{3^3},
\end{aligned} \tag{28}$$

$$\begin{aligned}
& A_j^{3d}(Q); \\
A_0^{3d}(Q) &= \left(\frac{253\,952}{55\,801\,305} + \frac{904\,192}{55\,801\,305} Q \right. \\
& \quad \left. + \frac{131\,072}{6\,200\,145} Q^2 \right) \frac{2^3}{3^3} Q^3, \\
A_1^{3d}(Q) &= \left(\frac{45\,056}{16\,740\,3915} + \frac{1\,440\,256}{18\,600\,435} Q \right. \\
& \quad \left. + \frac{149\,504}{6\,200\,145} Q^2 \right) \frac{2^3}{3^3} Q^2, \\
A_2^{3d}(Q) &= \left(\frac{140\,800}{3\,720\,087} + \frac{4\,211\,968}{6\,200\,145} Q + \frac{32\,768}{98\,415} Q^2 \right) \frac{2^3}{3^3} Q^2, \\
A_3^{3d}(Q) &= \left(\frac{2048}{885\,735} + \frac{2\,657\,792}{6\,200\,145} Q + \frac{48\,128}{32\,805} Q^2 \right) \frac{2^3}{3^3} Q, \\
A_4^{3d}(Q) &= \left(\frac{75\,008}{885\,735} + \frac{193\,472}{98\,415} Q + \frac{8192}{3645} Q^2 \right) \frac{2^3}{3^3} Q, \\
A_5^{3d}(Q) &= \left(\frac{256}{59\,049} + \frac{6304}{10\,935} Q + \frac{22\,912}{10\,935} Q^2 \right) \frac{2^3}{3^3}, \\
A_6^{3d}(Q) &= \left(\frac{736}{19\,683} + \frac{6416}{10\,935} Q \right) \frac{2^3}{3^3}, \\
A_7^{3d}(Q) &= \left(\frac{80}{2187} \right) \frac{2^3}{3^3}.
\end{aligned} \tag{30}$$

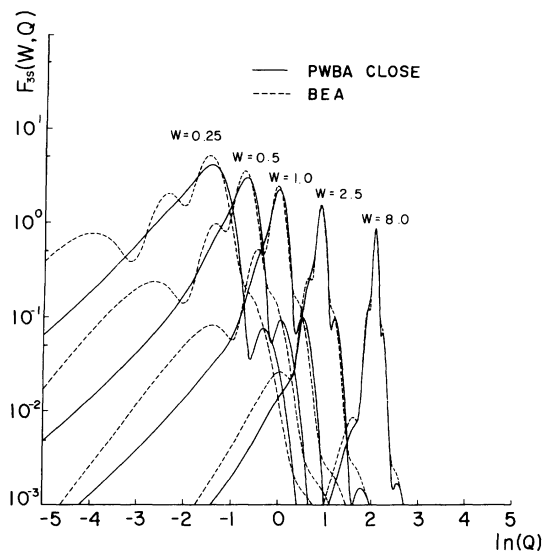
The generalized oscillator strengths calculated in terms of the impulse approximation $F_n^{\text{B}^j\text{EA}}(W, Q)$ are obtained from Eq. (6) by using the wave functions in momentum representation for the 3s, 3p, and 3d states as expressed by

$$\begin{aligned}
F_{3s}^{\text{B}^j\text{EA}}(W, Q) &= \frac{2^3}{\pi} W Q^{1/2} [(W - Q)^2 + \frac{4}{9} Q]^{-7} \\
& \quad \times \sum_{j=0}^8 [B_j^{3s}(Q)(W - Q)^j], \tag{31}
\end{aligned}$$

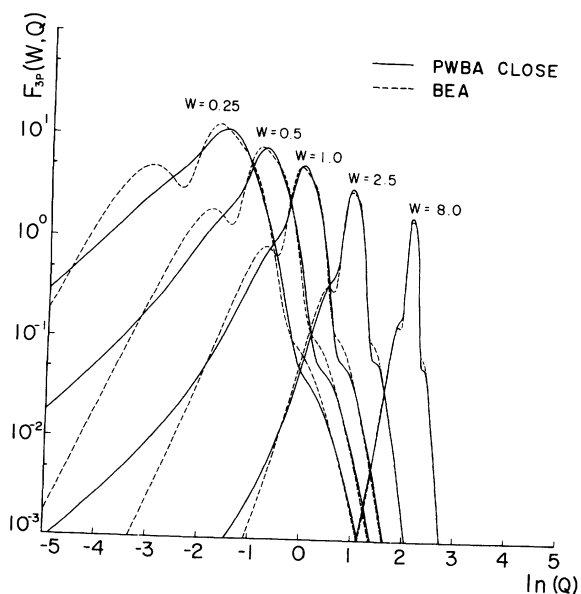
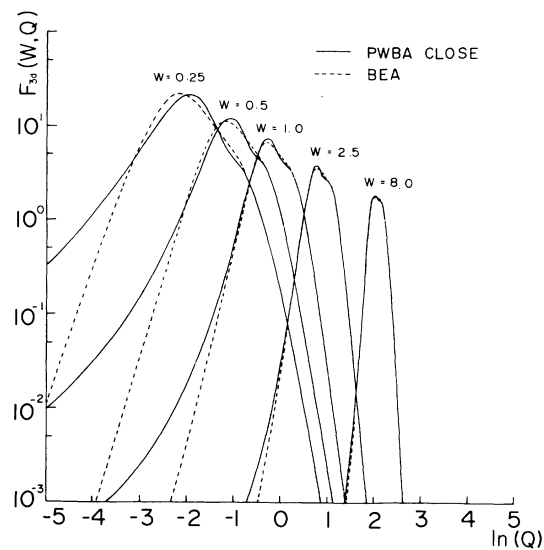
$$\begin{aligned}
F_{3p}^{\text{B}^j\text{EA}}(W, Q) &= \frac{2^3}{\pi} W Q^{1/2} [(W - Q)^2 + \frac{4}{9} Q]^{-7} \\
& \quad \times \sum_{j=0}^6 [B_j^{3p}(Q)(W - Q)^j], \tag{32}
\end{aligned}$$

$$\begin{aligned}
F_{3d}^{\text{B}^j\text{EA}}(W, Q) &= \frac{2^3}{\pi} W Q^{1/2} [(W - Q)^2 + \frac{4}{9} Q]^{-7} \\
& \quad \times \sum_{j=0}^4 [B_j^{3d}(Q)(W - Q)^j], \tag{33}
\end{aligned}$$

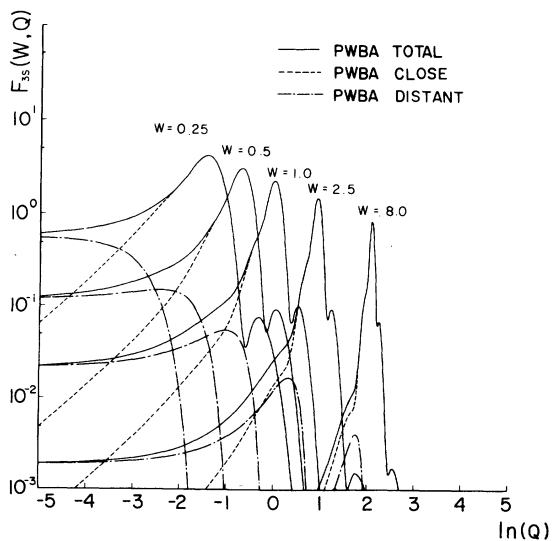
where the coefficients $B_j^{3s}(Q)$, $B_j^{3p}(Q)$, and $B_j^{3d}(Q)$ are given by

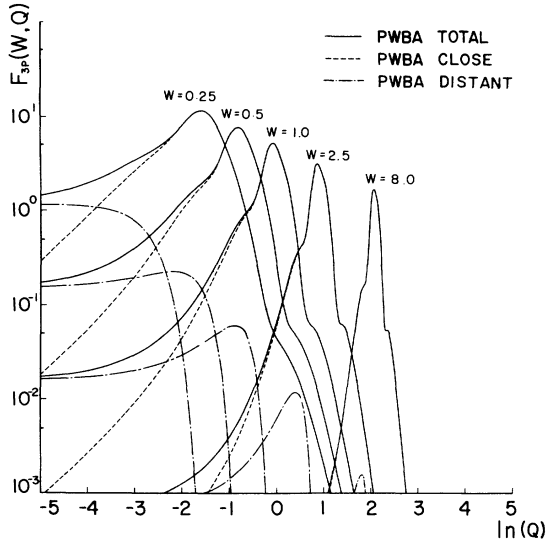
FIG. 9. Same as Fig. 3, except for the $3s$ state.
 $B_j^{3s}(Q):$

$$\begin{aligned}
 B_0^{3s}(Q) &= \left(\frac{68\,608}{6\,200\,145} Q^2 \right) \frac{2^3}{3^3} Q^3, \\
 B_2^{3s}(Q) &= \left(-\frac{17\,408}{98\,415} Q^2 \right) \frac{2^3}{3^3} Q^2, \\
 B_4^{3s}(Q) &= \left(\frac{15\,744}{10\,935} Q^2 \right) \frac{2^3}{3^3} Q, \\
 B_6^{3s}(Q) &= \left(-\frac{64}{27} Q^2 \right) \frac{2^3}{3^3}, \\
 B_8^{3s}(Q) &= \left(\frac{4}{3} Q \right) \frac{2^3}{3^3},
 \end{aligned} \tag{34}$$

FIG. 10. Same as Fig. 3, except for the $3p$ state.FIG. 11. Same as Fig. 3, except for the $3d$ state.
 $B_j^{3p}(Q):$

$$\begin{aligned}
 B_0^{3p}(Q) &= \left(\frac{8192}{413\,343} Q^2 \right) \frac{2^3}{3^3} Q^3, \\
 B_2^{3p}(Q) &= \left(\frac{2048}{6561} Q^2 \right) \frac{2^3}{3^3} Q^2, \\
 B_4^{3p}(Q) &= \left(-\frac{512}{243} Q^2 \right) \frac{2^3}{3^3} Q, \\
 B_6^{3p}(Q) &= \left(\frac{128}{27} Q^2 \right) \frac{2^3}{3^3},
 \end{aligned} \tag{35}$$

FIG. 12. Same as Fig. 5, except for the $3s$ state.

FIG. 13. Same as Fig. 5, except for the $3p$ state.

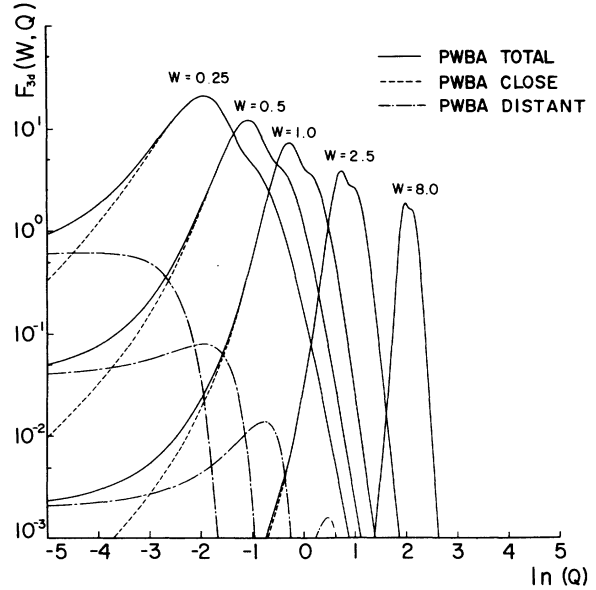
$B_j^{3d}(Q)$:

$$\begin{aligned} B_0^{3d}(Q) &= \left(\frac{131\,072}{6\,200\,145} Q^2 \right) \frac{2^3}{3^3} Q^3, \\ B_2^{3d}(Q) &= \left(\frac{32\,768}{98\,415} Q^2 \right) \frac{2^3}{3^3} Q^2, \\ B_4^{3d}(Q) &= \left(\frac{8192}{3645} Q^2 \right) \frac{2^3}{3^3} Q, \end{aligned} \quad (36)$$

where $B_j(Q)$ having odd j are zero.

Making a comparison between Eqs. (28)–(30) and Eqs. (34)–(36), we can find in the coefficients $A_j(Q)$ the terms corresponding to $B_j(Q)$ as in the case of L -shell ionizations. By using Eqs. (11)–(13) and Eqs. (24)–(30), we can calculate the close-collision part $F^{CC}(W, Q)$ and the distant-collision part $F^{DC}(W, Q)$ of the generalized oscillator strength for M shell. Figures 9, 10, and 11 show $F^{CC}(W, Q)$ for the $3s$, $3p$, and $3d$ states, respectively, calculated from Eqs. (31)–(33) and $F^{BEA}(W, Q)$. From the agreement between $F^{CC}(W, Q)$ and $F^{BEA}(W, Q)$ seen in these figures, the assumptions of Eqs. (11)–(13) are justified also for M -shell ionizations. Figures 12, 13, and 14 show $F^{CC}(W, Q)$ and $F^{DC}(W, Q)$, together with $F(W, Q)$. As seen in these figures, the behavior of $F^{DC}(W, Q)$ does not reflect the nodes of wave functions of the initial state of electron.

By using Eqs. (2), (11)–(13), and (24)–(30), we can obtain the ionization cross sections for the $3s$, $3p$, and $3d$ shells corresponding to close and distant collisions separately. In terms of these cross sections, the total M x-ray production cross sections are expressed by

FIG. 14. Same as Fig. 5, except for the $3d$ state.

$$\begin{aligned} (\sigma_X^{CC})_M &= \bar{\omega}_M \sum_{k=1} (\sigma_{i,k}^{CC})_M, \\ (\sigma_X^{DC})_M &= \bar{\omega}_M \sum_{k=1} (\sigma_{i,k}^{DC})_M, \\ (\sigma_X^{\text{total}})_M &= (\sigma_X^{CC})_M + (\sigma_X^{DC})_M. \end{aligned} \quad (37)$$

Here $\bar{\omega}_M$ is the average fluorescence yield for M shell and is taken to be 0.023 for Au and 0.035 for Bi from the table of Bambynek *et al.*,²⁹ and $\sigma_{i,k}$

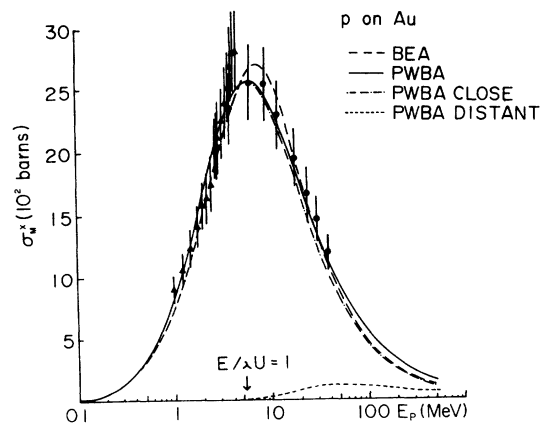


FIG. 15. The experimental M -shell ionization cross sections of Au for proton impact are compared with theoretical predictions from the BEA and PWBA. The PWBA cross sections are decomposed into the cross sections for close and distant collisions. The circles represent the present data and the triangles show the previous experimental results of Ref. 35.

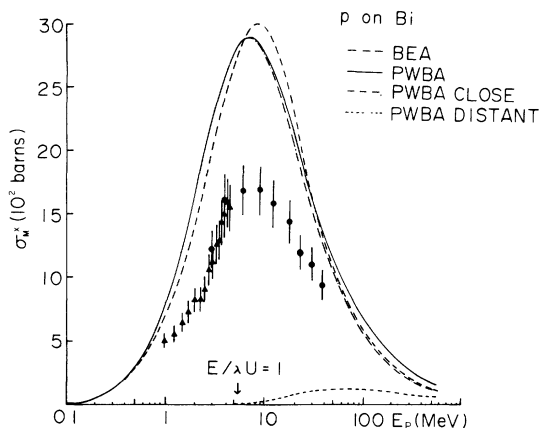


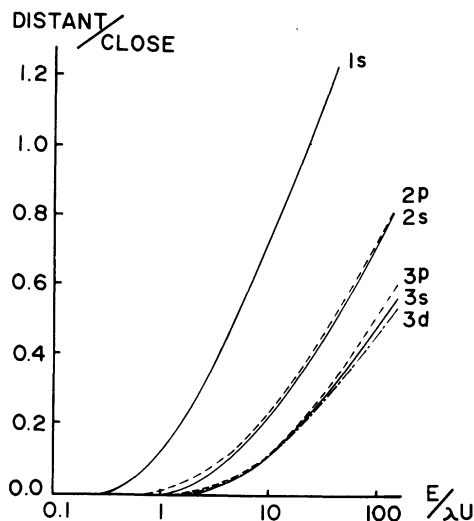
FIG. 16. Same as Fig. 17, except for Bi.

denotes the ionization cross section for a subshell M_k of the M shell. The results of calculation for Au and Bi are shown in Figs. 15 and 16, together with the present experimental results. These figures reveal that the contribution from distant collisions to the total ionization becomes still smaller than that for the L -shell ionization. However, contributions from distant and close collisions become again equal at very high projectile energy.

IV. RESULTS AND DISCUSSION

In the PWBA calculation of ionization cross sections, it is necessary to take account of the relativistic effect of inner-shell electrons or the screening effect. The electronic relativistic effect³⁰ becomes considerable only for heavy target atoms and low projectile energy, and this can be neglected in the present case. The screening effect has usually been brought into consideration by taking the effective nuclear charge.^{21, 26, 27} Furthermore, in some cases of direct Coulomb ionization, secondary effects such as increasing binding energy, Coulomb deflection, polarization, and inner-shell electron transfer to the projectile, considerably contribute to the cross section. These effects have been discussed and calculated in detail.^{10, 31, 32} In the present work, however, we are concerned with incident protons of velocity higher than that of inner-shell electrons to be ionized— $E/\lambda U > 1$ —and these effects can practically be neglected.⁵

Hence, the comparison between the nonrelativistic PWBA calculation and the experiment is discussed here. Theoretical predictions obtained using the values of fluorescence yield calculated by McGuire^{29, 33} are compared with the experimental results in Figs. 7 and 8, where the data on Y agree well with the PWBA, while those on Sn are in rather good agreement with the BEA. The ex-

FIG. 17. Ratio of cross sections for distant collisions to those for close collisions in K -, L -, and M -shell ionizations plotted as a function of $E/\lambda U$.

perimental results on Sn in the lower projectile-energy region, shown by triangles, have previously³⁴ been obtained. Comparisons between theories and experiments on the M -shell ionization of Au and Bi are illustrated in Figs. 15 and 16, where both the BEA and PWBA are in substantial agreement with the data on Au, while the theoretical values for Bi are 1.6 times larger than the experimental. This discrepancy seems to be due to an error in fluorescence yield, since the present experimental results are quite consistent with our previous results,³⁵ which have independently been determined with a Van de Graaff generator. Although the value of ω_M of Bi has been reported to be 0.037 ($\pm 19\%$) and 0.035 ($\pm 6\%$) by Jaffe³⁶ and Konstantinov,³⁷ respectively, an accurate re-determination of this quantity is desirable. In the figures, the cross sections predicted from the BEA at $E/\lambda U = 1$ are larger than those from the PWBA both in L - and M -shell ionizations as in the case of K -shell ionization,⁵ and the projectile energy corresponding to the maximum cross section is a little larger for the BEA than for the PWBA. The contribution from distant collisions to the L - and M -shell ionization cross sections in the energy range of $E/\lambda U = 1 \sim 10$ is not so large as in the case of K -shell ionization,⁵ and it seems that the contribution becomes smaller with the increase in the principal quantum number. Garcia pointed out that³⁸ the ionization cross sections for high-energy impact are in better agreement between the BEA and PWBA calculations with the increase in the principal quantum number, and this fact is quite consistent with the present result. Figure 17 shows the ratios of contribution between

close and distant collisions for various subshells plotted as a function of $E/\lambda U$. This figure reveals that the contribution from distant collisions depends primarily on the principal quantum number and is not sensitive to the azimuthal quantum number. Indeed, the ratio of the cross section for distant collisions to that for close collisions can be calculated as follows.

In a case where the projectile velocity is much greater than the velocity of inner-shell electrons, the inner-shell electrons can be regarded as free, and the ionization cross section for close collisions has been calculated in terms of BEA by³⁹

$$\sigma_n^{CC} = \pi \frac{z^2 e^4}{U_n^2} \frac{1}{E/\lambda U_n} \left(1 - \frac{1}{4} \frac{1}{E/\lambda U_n} \right), \quad (38)$$

where e is the electronic charge. On the other hand, the ionization cross section σ^{DC} for distant collisions is obtained from Eq. (2) by

$$\sigma_n^{DC} \approx \pi \frac{z^2 e^4}{U_n^2} \frac{1}{E/\lambda U_n} \ln \frac{4E}{\lambda U_n} \frac{1}{n^2} \int_{1/n^2}^{\infty} \frac{dW}{W} f_n(W), \quad (39)$$

where $f_n(W)$ denotes the optical oscillator strength for one electron. From Eqs. (38) and (39), the ratio of cross sections between distant and close collisions is calculated by

$$\frac{\sigma^{DC}}{\sigma^{CC}} = \ln \frac{4E}{\lambda U_n} \frac{1}{n^2} \int_{1/n^2}^{\infty} \frac{dW}{W} f_n(W). \quad (40)$$

In accordance with Bethe and Salpeter (see p. 208 of Ref. 26), an approximate expression of $f_n(W)$ for transitions between discrete states is given by

$$f_n(W) = \frac{1}{2n^2} \frac{1.96}{W^3 n^3}. \quad (41)$$

From this equation, Eq. (40) becomes

$$\frac{\sigma_n^{DC}}{\sigma_n^{CC}} \approx \frac{\ln(4E/\lambda U_n)}{3n}. \quad (42)$$

The principal-quantum-number dependence and the projectile-energy dependence of the ratio $\sigma_n^{DC}/\sigma_n^{CC}$, given by Eq. (42), are in substantial agreement with the present results.

The experimental errors in the present work are about 12%, while the errors in relative cross sections are only ~2%, so that the experimental projectile-energy dependence of the x-ray production cross sections can be compared with theoretical predictions more accurately than the absolute cross sections. This comparison can be done in terms of least-squares method by

$$\sigma_\lambda = \left[\frac{1}{N} \sum_i \left(1 - \lambda \frac{\sigma_{\text{theor}}^x(E_i)}{\sigma_{\text{expt}}^x(E_i)} \right)^2 \right]^{1/2}$$

with

$$\lambda = \frac{\sum_i \left(\frac{\sigma_{\text{theor}}^x(E_i)}{\sigma_{\text{expt}}^x(E_i)} \right)}{\sum_i \left(\frac{\sigma_{\text{theor}}^x(E_i)}{\sigma_{\text{expt}}^x(E_i)} \right)^2}, \quad (43)$$

where $\sigma_{\text{theor}}^x(E_i)$ and $\sigma_{\text{expt}}^x(E_i)$ are, respectively, the theoretical and experimental x-ray production cross sections at an incident energy E_i . Since we are here interested in the region of $E/\lambda U > 1$, the data only in this region are summed up in Eq. (43), and N is the number of data which are summed up. Hence, σ_λ means the degree of agreement of the projectile-energy dependence of x-ray production cross section between the experiment and the theoreticals $\sigma_{\text{PWBA}}^{\text{total}}$, $\sigma_{\text{PWBA}}^{\text{CC}}$, and σ^{BEA} , and λ is the fitting parameter. The values of σ_λ are shown in Table II for L shells of Y and Sn and M shells of

TABLE II. Least-squares fitting of projectile-energy dependence of the x-ray production cross sections between the experimental results and the theoretical predictions $\sigma_{\text{PWBA}}^{\text{total}}$, $\sigma_{\text{PWBA}}^{\text{CC}}$, and σ^{BEA} . The values of σ_λ , defined by Eq. (44), represent the degree of agreement between the theory and the experiment.

	Y-L		Sn-L		Au-M		Bi-M	
	$\sigma_{\lambda=1}$		$\sigma_{\lambda=1}$		$\sigma_{\lambda=1}$		$\sigma_{\lambda=1}$	
$\sigma_{\text{PWBA}}^{\text{total}}$	0.17		0.097		0.056		0.59	
$\sigma_{\text{PWBA}}^{\text{CC}}$	0.055		0.157		0.101		0.55	
σ^{BEA}	0.25		0.0105		0.053		0.66	
	σ_λ	λ	σ_λ	λ	σ_λ	λ	σ_λ	λ
$\sigma_{\text{PWBA}}^{\text{total}}$	0.014	0.86	0.0093	1.11	0.028	1.05	0.048	0.63
$\sigma_{\text{PWBA}}^{\text{CC}}$	0.052	0.98	0.023	1.18	0.054	1.09	0.074	0.65
σ^{BEA}	0.051	0.81	0.0081	0.993	0.048	1.01	0.54	0.60

Au and Bi. The degree of agreement of absolute cross sections between the experiment and the theories, which is given by the values of σ_λ for $\lambda=1$, is also shown. These values explain quite well the results obtained from comparisons between the experiment and the theories shown in Figs. 7, 8, 15, and 16; the value of σ_λ is the least for σ_{PWBA}^{total} in all the elements, and the deviation of λ from unity, except for Bi, is less than $\sim 10\%$, which is consistent with our experimental errors of $\pm 12\%$. A clear difference in σ_λ is seen between σ_{PWBA}^{total} and σ_{PWBA}^{CC} , especially in cases of Y-*L* and Au-*M* values. This fact proves the contribution from distant collisions to *L*- and *M*-shell ionizations in the energy region of $E/\lambda U = 1-10$, and also the fairly good agreement of σ_λ between σ_{PWBA}^{CC} and σ^{BEA} shows the same projectile-energy dependence, which can be understood from discussions given above.

V. SUMMARY

The total x-ray production cross sections for *L*-shell ionizations of Y and Sn and for *M*-shell ionizations of Au and Bi have been measured for 3–40-MeV proton impact— $E/\lambda U = 0.4-10$. Inner-

shell ionizations by close and distant collisions have been discussed on the basis of the generalized oscillator strength and the general formulas for inner-shell ionization by these two kinds of collisions have separately been derived from the PWBA theory. The experimental results, except those for Bi *M*-shell ionizations, were in agreement with the PWBA and BEA calculations within $\sim 10\%$. The projectile-energy dependence of the cross sections proved that the distant collision surely contributes to the *L*- and *M*-shell ionizations, but is not as remarkable as in the *K*-shell ionization in agreement with the theoretical prediction.

ACKNOWLEDGMENTS

The authors wish to express their sincere thanks to Mr. Hoshika, Mr. Ohmura, Mr. Ono, and Mr. Kan for operating the cyclotron throughout the experiment and also to Mr. Sugai of the Institute for Nuclear Study of Tokyo University for the support and cooperation in the target-thickness measurement with the α -ray thickness gauge.

- ¹E. Merzbacher and H. W. Lewis, in *Encyclopedia of Physics*, edited by S. Flügge (Springer, Berlin, 1958), Vol. 34, p. 166.
- ²J. D. Garcia, *Phys. Rev. A* **1**, 280 (1970).
- ³J. M. Hansteen and O. P. Mosebekk, *Nucl. Phys. A* **201**, 541 (1973).
- ⁴G. Bissinger, J. M. Joyce, B. L. Doyle, W. W. Jacobs, and S. M. Shafroth, *Phys. Rev. A* **16**, 443 (1977).
- ⁵K. Sera, K. Ishii, M. Kamiya, A. Kuwako, and S. Morita, *Phys. Rev. A* **21**, 1412 (1980).
- ⁶G. A. Bissinger, J. M. Joyce, E. J. Ludwig, W. S. McEver, and S. M. Shafroth, *Phys. Rev. A* **1**, 841 (1970).
- ⁷G. Bissinger, J. M. Joyce, and H. W. Kugel, *Phys. Rev. A* **14**, 1375 (1976).
- ⁸T. L. Hardt and R. L. Watson, *Phys. Rev. A* **7**, 1917 (1973).
- ⁹W. D. Ramsay, M. S. A. L. Al-Ghazi, J. Birchall, and J. S. C. Mckee, *Phys. Lett.* **69A**, 258 (1978).
- ¹⁰G. Basbas, W. Brandt, and R. Laubert, *Phys. Rev. A* **17**, 1655 (1978).
- ¹¹G. A. Bissinger, S. M. Shafroth, and A. W. Waltner, *Phys. Rev. A* **5**, 2046 (1972).
- ¹²R. L. Watson, C. W. Lewis, and J. B. Natowitz, *Nucl. Phys.* **A154**, 561 (1970).
- ¹³T. L. Hardt and R. L. Watson, *Phys. Rev. A* **14**, 137 (1976).
- ¹⁴T. L. Hardt and R. L. Watson, *At. Data Nucl. Data Tables* **17**, 107 (1976).
- ¹⁵N. Maeda, N. Kobayashi, H. Hori, and M. Sakisaka, *J. Phys. Soc. Jpn.* **40**, 1430 (1976).
- ¹⁶C. E. Busch, A. B. Baskin, P. H. Nettles, S. M. Shafroth, and A. W. Waltner, *Phys. Rev. A* **6**, 1601 (1973).
- ¹⁷M. Poncet and C. Engelmann, *Nucl. Instrum. Methods* **149**, 461 (1978).
- ¹⁸M. Poncet and C. Engelmann, *Nucl. Instrum. Methods* **159**, 455 (1979).
- ¹⁹I. Nonaka and I. Sugai, Report No. INS-J-132, 1971 (unpublished).
- ²⁰H. Kolbenstvedt, *J. Appl. Phys.* **38**, 4785 (1967).
- ²¹Byung-Ho Choi, *Phys. Rev. A* **7**, 2056 (1973).
- ²²H. Bethe, *Ann. Phys. (Leipzig)* **5**, 325 (1930).
- ²³M. Inokuti, *Rev. Mod. Phys.* **43**, 297 (1971).
- ²⁴L. Vriens and T. F. M. Bensen, *J. Phys. B* **1**, 1123 (1968); L. Vriens, in *Case Studies in Atomic Collision Physics I*, edited by E. W. McDaniel and M. R. C. McDowell (North-Holland, Amsterdam, London, 1969), p. 335.
- ²⁵A. Bethe and E. E. Salpeter, *Quantum Mechanics of One- and Two-Electron Atoms* (Plenum, New York, 1977), p. 36.
- ²⁶Byung-Ho Choi, *Phys. Rev. A* **4**, 1002 (1971).
- ²⁷B. H. Choi, E. Merzbacher, and G. S. Khandelwal, *At. Data* **5**, 291 (1973).
- ²⁸O. Benka and A. Kropf, *At. Data Nucl. Data Tables* **22**, 219 (1978).
- ²⁹W. Bambynek, B. Crasemann, R. W. Fink, H. U. Freund, H. Mark, C. D. Swift, R. E. Price, and P. V. Rao, *Rev. Mod. Phys.* **44**, 716 (1972).
- ³⁰M. Kamiya, K. Ishii, K. Sera, S. Morita, and H. Tawara, *Phys. Rev. A* **16**, 2295 (1977).
- ³¹W. Brandt and G. Lapicki, *Phys. Rev. A* **20**, 465 (1979).

- ³²J. F. Reading, A. L. Ford, and E. Fitchard, Phys. Rev. Lett. 36, 573 (1979).
- ³³E. J. McGuire, Phys. Rev. A 3, 1801 (1971).
- ³⁴K. Ishii, S. Morita, H. Tawara, H. Kaji, and T. Shio-kawa, Phys. Rev. A 10, 774 (1974).
- ³⁵K. Ishii, S. Morita, H. Tawara, H. Kaji, and T. Shio-kawa, Phys. Rev. A 11, 119 (1975).
- ³⁶H. Jaffe, University of California Lawrence Radiation Laboratory Report No. UCR-2537, 1954 (unpublished).
- ³⁷A. A. Konstantinov and T. E. Sazonova, Izv. Akad. Nauk. SSSR Ser. Fiz. 32, 631 (1968) [Bull. Acad. Sci. USSR Phys. Ser. 32, 581 (1968)].
- ³⁸J. D. Garcia, Phys. Rev. 159, 39 (1967).
- ³⁹T. F. M. Bensen and L. Vriens, Physica (Utrecht) 47, 307 (1970).